Antarctic polar stratospheric cloud composition as observed by ACE, CALIPSO and MIPAS

Léo Lavy[a,*], Peter Bernath[a,b,c], Michael Lecours[b] and Dylan English[c]

[a]*Department of Chemistry and Biochemistry, Old Dominion University, Norfolk, VA 23529, USA*

[b]*Department of Chemistry, University of Waterloo, Waterloo, ON N2L3G1, Canada*

[c]*Department of Physics, Old Dominion University, Norfolk, VA 23529, USA*

[*]*Corresponding author. E-mail address: llavy@odu.edu*

Abstract

The composition of polar stratospheric clouds (PSCs) in the Antarctic is measured by infrared absorption spectroscopy by the Atmospheric Chemistry Experiment (ACE) satellite and compared to lidar (CALIPSO) and emission spectroscopy (MIPAS) results. ACE observations are compared first to CALIPSO for the period 2006-2020, then to MIPAS for the period 2005-2011, and then a set of triple coincidences is studied. In both CALIPSO-ACE and MIPAS-ACE comparisons, nitric acid trihydrate (NAT) detections are in excellent agreement (~80% of coincident compositions is found). Supercooled ternary solution (STS) detections are in good agreement for CALIPSO-ACE (~60%) but in poor agreement for MIPAS-ACE (39%). This contrasts with ice detections, in poor agreement for CALIPSO-ACE (~30%) and in better agreement for MIPAS-ACE (45%). Triple coincidences show that ACE STS detections are more reliable than MIPAS STS detections. ACE observations compared to homogeneous CALIPSO PSCs show that for 11 observations, CALIPSO is observing supercooled nitric acid (SNA) clouds rather than STS clouds.

Keywords (max 6)

Atmospheric Chemistry Experiment, CALIPSO, MIPAS, Polar stratospheric clouds, Infrared solar absorption spectroscopy, satellite remote sensing.

1. Introduction

Polar stratospheric clouds (PSCs) form in the polar vortex when the temperature drops below about 195 K [1,2]. They occur every winter and are particularly prominent over Antarctica. These clouds are important because they catalyze chemical reactions leading to the depletion of stratospheric ozone. Chlorine and bromine atoms released in the stratosphere by photolysis of anthropogenic CFCs (chlorofluorocarbons) and halons are the main actors in ozone depletion [3]. These atoms can form reservoir molecules (e.g., HCl, $ClONO_2$) that do not destroy ozone [4]. However, chemistry on the surface (or in the interior) of PSC particles, and subsequent photolysis release deleterious chlorine and bromine atoms again, as observed first in the Antarctic [5,6]. Denitrification of the stratosphere also affects ozone. Denitrification is caused by condensation of nitrate-containing species on PSCs followed by sedimentation of these particles; in this way, NO_2 concentrations decrease, delaying the recovery of polar ozone by slowing the reformation of

$ClONO_2$. A decline in the concentration of HNO_3 vapor can be used to infer the presence of PSCs [7].

PSCs are liquid and solid particles in the stratosphere and gas-phase molecules interact with them in many ways, including condensation and chemical catalysis. Laboratory experiments have measured the kinetics of heterogeneous reactions on PSC particles [8]. Models help to explain PSC chemical composition (e.g., thermodynamics [9]) and provide insight on the chemistry of chlorine-containing species on PSCs (e.g., chemical model CLaMS [10]). Current models of polar ozone chemistry need to take PSCs into account to make correct predictions [11].

Characterization of PSCs is important because size, chemical composition, and phase of the particles influence chemistry. Measurement methods used to detect PSCs include aircraft missions [12,13], balloon borne instrumentation [14], ground based lidars [15–17], and satellites, allowing them to be studied in detail [2,18–20]. Based on observations and models, PSC chemical composition was found to be three main types: supercooled droplets of ternary solutions with sulfuric acid, nitric acid, and water (STS), solid crystals of nitric acid trihydrate (NAT, in the crystal form of β-NAT) and ice particles. Spectroscopic signatures of PSCs from absorption spectroscopy observations of the Atmospheric Chemistry Experiment (ACE) satellite demonstrate that supercooled nitric acid (SNA) droplets are present in the clouds [21]; this was also measured earlier by the ILAS-II satellite instrument [22].

Solar occultation satellites such as SAM II [23], the SAGE series [24,25], and the POAM series [26,27] laid the groundwork for much of our early knowledge on PSCs. The most recent satellite observations of PSCs were made by MIPAS (Michelson Interferometer for Passive Atmospheric Sounding) (2002-2012) instrument on ENVISAT, CALIPSO (Cloud-Aerosol Lidar and Infrared Pathfinder Satellite Observations) (2006-2023) and ACE (2003-present). These three satellites/instruments use different physical phenomena to detect PSCs: infrared emission of the limb of the atmosphere, backscattered light and depolarization ratio with lidar, and infrared transmittance of the limb during sunsets and sunrises. The ACE mission is the only satellite still operating today and it spans the lifetimes of MIPAS and CALIPSO almost entirely, allowing a detailed comparison of PSCs observed by the three different methods. In this work, the previous comparison between CALIPSO and ACE [28] is extended and a comparison between MIPAS and ACE is added.

2. Methods

2.1. ACE

ACE is a satellite mission onboard the Canadian satellite SCISAT. It was launched by NASA on August 12, 2003 and has been operational ever since. At launch it orbited at an altitude of 650 km with 74° inclination to the equator. The primary instrument is a high-resolution (0.02 cm^{-1}) Fourier Transform Spectrometer (FTS) operating within the spectral range of 750–4400 cm^{-1} (2.2–13.3 μm) [29]. In this paper, we will refer to the ACE-FTS instrument and the satellite as "ACE". The FTS captures 30-40 atmospheric transmittance spectra per occultation, during sunrise and sunset in a limb geometry (solar occultation). These spectra are processed on the ground [30], and altitude-dependent concentration profiles are obtained [31]. Based on the HITRAN2020 database

[32], molecular signatures are removed, and residual spectra of clouds and aerosols obtained [33]. Spectral simulations identify key features in these spectra to characterize PSCs [21]. ACE has a circular field of view of 1.25 mrad, corresponding to a spatial resolution of 3-4 km at the limb. The horizontal resolution along the line of sight is about 400 km and the vertical sampling varies between 2 and 6 km [Bernath 2017]. The tangent point can move as far as ~300 km during an occultation between the lowest and highest observed PSC, but it moves less than 50 km in most cases. For simplicity, a median tangent point of the observations was considered for coincidence finding.

For the present work, the latest version of ACE-FTS processing (v5.2) is used [34] in order to create PSC profiles and the PSC composition dataset is the same as used previously [20]. Briefly, the classification scheme uses five categories: NAT, STS, NAT-STS, ice-mixture, and SNA. One must keep in mind that these categories are based on the most prominent features and typically the spectra have a mixed character. Ice for example is almost always found mixed with some NAT and STS, so no pure ice categories are considered. The NAT-STS category was initially created for spectra that present features from both NAT and STS. However, upon more careful inspection some of these spectra might also be the signature of large NAT particles, therefore this category might evolve in the future. Also, because ACE-FTS measures the atmospheric limb, there can be more than one cloud along the line-of-sight, resulting in a mixed spectrum. ACE is not able to distinguish between internal (one particle) and external mixtures (two clouds along the line-of-sight) unless they interact spectroscopically. It is possible and likely that many of our mixtures are one PSC near the tangent height and another at higher altitudes in the foreground or background of the measurement. SNAs are rare and represent less than 0.5% of the total number of PSCs in this study. They still are important to study because they hint at increased aerosol size and they control freezing properties, therefore impacting the formation of PSCs and extent of seasonal ozone depletion. ACE is also able to detect sulfate aerosols, and a substantial number were detected during the Antarctic winter as explained in reference [20]. We found in this study that sulfate detection by ACE results in no-cloud detection by MIPAS or CALIPSO in more than 90% of cases.

PSC composition is detected by ACE with unambiguous spectral features in the FTS spectral range, e.g., nitrate bands at 820 cm^{-1} and 1350 cm^{-1}, OH stretching bands near 3300 cm^{-1}, nitric acid bands at 1420 cm^{-1} and 1720 cm^{-1} and upward ice features at 1000 cm^{-1} and 3550 cm^{-1} [33,21]. Antarctic PSC composition is analyzed from 2005 to 2023 in reference [20] and was compared to CALIPSO for a small period [28].

2.2. CALIPSO

CALIPSO is a joint satellite mission between NASA and the French space agency (CNES) within the Earth Observing System program. It was originally part of the A-train [35], a constellation of satellites for the observation of the Earth's atmosphere. CALIPSO mission started in 2006 and ended in 2023. CALIPSO orbited at an altitude of 700 km with 98° inclination to the equator. Its principal instrument is a lidar called CALIOP (Cloud-Aerosol Lidar with Orthogonal Polarization) [36]. CALIOP uses a polarized laser with a principal wavelength in the green (532 nm) oriented in the nadir direction. The laser is pulsed and generates a full vertical profile every 50 ms, which corresponds to 335 m along the ground. This results in high spatial resolution along the satellite

ground track, and with 14-15 orbits per day, CALIPSO gives unique spatial coverage. We will refer the satellite and the CALIOP lidar simply as "CALIPSO".

PSCs are observed by CALIPSO as enhancement in the total backscattered light with possible depolarization at 532 nm as studied by Pitts et al. [19,37–40]. Ice and NAT particles, because of their irregular shape, depolarize the return signal. On the other hand, liquid particles such as STS are spherical, and the backscattered light keeps its initial polarization. For this study we used the latest PSC data product, with observations limited to nighttime, available through NASA Earth Observation Data website (https://www.earthdata.nasa.gov/), namely the CALIPSO Lidar Level 2 Polar Stratospheric Clouds data product. It uses the PSC detection and composition classification algorithm described by Pitts et al. [19] that also relies on Aura MLS measurements of PSC condensable vapors HNO_3 and H_2O. This data product considers the following PSCs compositions: ice, wave-ice (ice PSCs typically induced by mountain-waves), NAT, enhanced-NAT (subcategory of NAT with higher number densities of NAT particles) and STS. Some tropospheric clouds are also reported. As for ACE, these categories are named based on the main character of the observation and in general the PSCs are mixtures. NAT composition classification represents mixtures of NAT and liquid particles (either background sulfate or STS, depending on temperature). The STS classification also may include NAT particles that are not detected by CALIPSO.

2.3. MIPAS

MIPAS is a mid-infrared emission spectrometer onboard the satellite ENVISAT, measuring infrared spectra in the 685 to 2070 cm^{-1} (4.15–14.6 μm) range [41]. It orbited the Earth and took data from July 2002 to April 2012, at an altitude of about 785 km and with 98.6° inclination to the equator. Throughout this paper, we will refer to the instrument and the satellite as "MIPAS". MIPAS scans the limb and measures thermal emission spectra of the atmosphere. MIPAS field of view is rectangular with vertical extent of ~3 km and horizontal extend of ~30 km at the limb. As for ACE, the horizontal resolution along the line of sight is about 400 km [2].

The classification of PSCs was mainly developed by Spang et al. [42–45,18] and the latest work uses a database of modeled spectra for homogeneous layers with a single PSC composition. Similar to ACE, most PSCs are found to be mixtures of the basic PSC types. The compositions are defined as the most dominant PSC type in the modeled radiance of the spectra. The MIPAS PSC climatology over the full length of the mission was studied by Spang et al. [18], and a study of gravity wave-induced PSCs was made by Hoffmann [46]. In our work, MIPAS data available online (https://datapub.fz-juelich.de/slcs/mipas/psc/) were used [47] and were obtained with the Bayesian-based composition classification algorithm detailed in references [18,45]. The algorithm assigns a probability for each composition that contributes to the PSC spectra. This data product includes the following PSC compositions: ice, NAT, STS (pure PSCs are assumed when the probability is over 50%), NAT-STS (when the probability of NAT and STS are both between 40 and 50%), unknown (when the probability of ice, NAT and STS are all below 40%), ice-NAT, ice-STS (the last two classifications are not found in our set of coincidences).

For MIPAS, the most prominent feature in the spectra is the nitrate band at 820 cm^{-1} and is characteristic of β-NAT PSCs. For other PSCs, the classification relies on spectral shape (gradient from 830 to 940 cm^{-1} for ice and constant baseline for STS [2]). This contrasts with ACE which uses several characteristic bands for each PSC and covers the important OH stretching region near 3000 cm^{1}. Absorption spectra are also easier to interpret than emission spectra because absorption spectral simulations use only the Beer-Lambert law. Solar occultation is potentially more sensitive to optically thin clouds than MIPAS, as found by earlier comparison of MIPAS with solar occultation satellites SAGE III and POAM III [43].

2.4. Data sets

In this paper, the same ACE data set as in reference [20] is used. As shown in Figure 6 of reference [29], the sampled latitude of the ACE satellite is a function of the time of the year. We used ACE observations between 75°S and 83°S which correspond exclusively to sunset observations over the Antarctic, roughly between the last week of August to the third week of September.

The Fig. 1 (a) shows on a map the ACE observations for 2010 in the Antarctic. The dots represent 1° latitude and 10° longitude regions and are colored according to the number of profiles containing PSCs in that region. Fig. 1 (b) shows ACE observations of PSCs considered in this paper for 2010, in the period 8-25-2010 to 9-19-2010. ACE spatial coverage is compared to CALIPSO spatial coverage in Fig. 1 (c) and MIPAS spatial coverage in Fig. 1 (d) for the same 2010 period. CALIPSO measures many profiles in the nadir direction along its track; the number of CALIPSO observations near 82°S is particularly large. In contrast to the two other satellites, MIPAS can measure profiles at very high latitudes. Unlike ACE, MIPAS is independent of light sources and therefore has more observations.

Before presenting the comparisons, we will highlight the differences in measurement between the three satellites, as it influences the interpretation of the results. CALIPSO is a nadir viewing satellite with high vertical and horizontal resolution, which contrasts with limb viewing satellites ACE and MIPAS. Limb viewing satellites have a large field of view that can cover several CALIPSO observations, and the line of sight crosses different altitudes. A limb viewing observation is associated with the tangent altitude but rigorously, the observed cloud could be situated anywhere in the line of sight. Considering an extreme case: a limb observation at 9 km tangent altitude could be caused by a cloud at 25 km altitude, 350 km away from the tangent point. Unfortunately, there is no easy way to determine if the observation corresponds to a cloud near the tangent altitude or far from it; but clouds at the tangent altitude contribute more to the optical thickness. Concerning the actual characterization of clouds, it is important to note that although CALIPSO has a high spatial resolution, the characterization relies only on backscattered light and depolarization, which is less accurate than the spectroscopic observations made by ACE and MIPAS. The comparisons of this article will be centered around the observations of ACE, as these are the most reliable composition measurements.

3. Results

3.1. CALIPSO-ACE coincidences

The ACE data set was compared with CALIPSO between 2006 and 2020. Coincidences were found using the same criteria as in the previous study [28] ($\Delta t \leq 6$ hours and $\Delta d \leq 150$ km). It is important to note that for most coincidences CALIPSO measures at least 1 h after ACE. Table 1 shows the number of coincident profiles for each year. It also shows the number of individual PSCs detected by ACE and their composition.

The ACE data set contained, on average, 237 ACE occultations per year [20]. On average, 174 were found in coincidence with a CALIPSO profile. The number of ACE detections can vary up to a factor of two from year to year. The most detected type of PSC is NAT-STS mixtures. The rest of PSC detections are distributed, in order of importance, between NAT, STS and ice. Over the whole coincidence data set there were 45 SNA detections, which is more significant than in our previous study.

The comparison between ACE and CALIPSO is done the same way as the previous comparison [28]. Briefly, the ACE composition was compared with the closest CALIPSO vertical profile and CALIPSO observations were integrated in a 4 km vertical window for each ACE data point, without taking into account CALIPSO no-cloud detections. Considering CALIPSO vertical resolution of 180 m, this means that up to 23 CALIPSO measurements can be compared to a single ACE measurement, and these are all added into the comparison histograms. Fig. 2 shows for each PSC composition detected by ACE, the ratio of each CALIPSO classification as a function of the year. Similar trends as those found in the previous analysis are reported here, i.e., $77 \pm 7\%$ of ACE NAT detections are also detected as NAT by CALIPSO, about $62 \pm 9\%$ of ACE STS detections are also detected as STS by CALIPSO and about $27 \pm 6\%$ of ACE ice-mix detections are detected as ice by CALIPSO (one standard deviation is reported as uncertainties). These percentages are roughly constant from 2006 to 2020. These ratios must be considered together with the number of events used in the statistics for each year (Table 1). Another important result found here, with more confidence than in the previous study, is the detection of ACE SNA PSCs as STS by CALIPSO. The identification of SNA clouds as STS by CALIPSO is not surprising since both particles are liquid, and likely cannot be distinguished with lidar. This study shows that the CALIPSO STS category contains a small percentage of SNA, i.e. particles with lower sulfuric acid content than expected. Finally, ACE NAT-STS is detected by CALIPSO either as NAT or as STS. This is a good agreement considering that CALIPSO NAT classification is defined as a mixture of NAT particles and liquid droplets and CALIPSO STS classification may also include mixtures of STS and low number densities of NAT particles.

Coincidences between MIPAS and CALIPSO were analyzed previously, using only CALIPSO's homogeneous cloud detection [2]. A similar comparison was carried out in our work between ACE and CALIPSO. The original study determined homogeneous clouds based on a 200 km horizontal by 3 km vertical box of CALIPSO observations. With this method, our analysis suffers from too low statistics, therefore, only a single vertical slice of CALIPSO data was considered (the closest profile). PSC scenes were considered homogeneous when more than 50% of the observations within a 4 km vertical window around the ACE observation were PSCs according to CALIPSO and more than 75% of these PSCs belong to a single CALIPSO composition. Fig. 3 shows for each CALIPSO homogeneous composition, the associated ACE compositions. The agreement between

the two satellites improves compared to the first analysis, especially for ice (37% agreement) and STS (69% agreement). However, the agreement for ice is not nearly as good as the almost perfect agreement found in MIPAS-CALIPSO comparison [2]. It must be noted that [2] used more stringent coincidence criteria ($\Delta t \leq 1$ hours and $\Delta d \leq 100$ km) compared to ours ($\Delta t \leq 6$ hours and $\Delta d \leq 150$ km). In our case, the use of $\Delta t \leq 3$ hours $\Delta d \leq 100$ km reduced the total coincidences from 2619 to 404 and no significant changes in the statistics were found. It is worth noting that all the 11 SNA detections by ACE correspond to homogeneous STS scenes according to CALIPSO.

3.2. MIPAS-ACE coincidences

ACE PSC composition was compared with MIPAS from 2005 to 2011. The same coincidence criteria as before were used ($\Delta t \leq 6$ hours and $\Delta d \leq 150$ km). The composition of ACE is compared with the closest altitude MIPAS detection. Using this method, about 30% of ACE PSCs were associated with a no-cloud detection for MIPAS, no matter the PSC composition. This number is similar to the amount of ACE PSCs with no-cloud detection by CALIPSO found previously (23% [28]). This discrepancy can be due to the spatial variability of the clouds and the fact that the line-of-sight of the two satellites are not aligned in most cases. These events are disregarded for the present analysis. Both ACE and MIPAS satellites are moving while scanning the limb of the atmosphere. This results in the tangent points being different at all altitudes. For simplicity, the median tangent point of the altitudes is used to determine coincidences. For almost 90% of the coincidences, MIPAS measures at least 4 hours before ACE, and this bias is worth noting. The distance between the two satellite observation locations on the other hand is not significantly biased.

Overall, 209 coincident profiles were found, corresponding to 701 coincident PSC detections. The composition comparison is shown in Fig. 4. The agreement for ice cloud detections between ACE and MIPAS (45%) is better than between ACE and CALIPSO (30%, Fig. 2). The agreement for NAT PSCs is very good (82%), as before with CALIPSO. The satellite detections for STS are in poor agreement: 39% of ACE STS were classified as STS by MIPAS, while 51% were classified as NAT. This contrasts with the CALIPSO-MIPAS comparison [2], for which most of CALIPSO STS homogeneous detections were classified as STS or NAT-STS by MIPAS. However, this MIPAS-CALIPSO comparison is based on more STS observations (562) than our MIPAS-ACE comparison (74).

3.3. CALIPSO-MIPAS-ACE coincidences

Lastly, we studied triple coincidences CALIPSO-MIPAS-ACE. Here, triple coincidences mean coincidences for which observations of CALIPSO and MIPAS happened less than 6 hours and 150 km relative to ACE, not relative to each other. CALIPSO and MIPAS observations can therefore be up to 12 hours and 300 km apart during a so-called triple coincidence. A total of 162 such coincidences were found between 2006 and 2011. MIPAS measures between 7 and 9 hours before CALIPSO for 90% of those with a spatial separation of less than 150 km 75% of the time. The Fig. 5 shows on an Antarctic map the ACE observations for this period (black dots) and the ACE observations found in triple coincidence (color dots). The triple coincidences are colored according to the day of the year, triangles represent events in August and circles in September. The

number of triple coincidences is shown next to the year. Our set of triple coincidences is very localized in latitude as seen in the figure.

An example of a triple coincidence is shown in Fig. 6. This shows the detection of an ice PSC by CALIPSO that spans several thousand kilometers and was detected in 4 consecutive CALIPSO orbits (more than 5 hours). Each orbit was coincident with ACE observations (circles) and MIPAS observations (triangles). Faint grey curves show the line-of-sight of the ACE satellite. Here, both limb viewing satellites detect ice in these coincidences, in excellent agreement with the lidar. The ACE measurement is above the cloud altitude reported by CALIPSO. ACE can only measure spectra if the PSCs are optically thin enough for sunlight to pass through, so in these occultations we are not able to retrieve below this altitude. MIPAS, on the other hand, reports measurements in the middle altitude of the cloud. MIPAS is an emission spectrometer and does not have such a limitation. The tendency of ACE to detect ice at the edge of the cloud (where the optical thickness is small) could partly explain the CALIPSO-ACE disagreement for ice. Indeed, the Figure shows that the edge of the cloud is identified as NAT or STS in the CALIPSO dataset and that there is rarely a sharp separation between ice and no-cloud. Overall, the figure shows that a very large and persistent ice cloud is clearly identified by the three satellites.

Fig. 7 shows the comparison between the PSC composition of all three satellites for these triple coincidences. A pie chart of CALIPSO compositions is shown for each ACE-MIPAS pair of compositions and the number of such pairs is shown in the corner. We find again that ACE and MIPAS are in good agreement for NAT (120 coincident detection of NAT clouds) but in poor agreement for STS (19 coincident detection of STS clouds). For the row of ACE STS detections, the pie charts show that CALIPSO detects mostly STS. On the other hand, looking at the column of STS for MIPAS, the majority of those are detected as NAT by CALIPSO. Therefore, ACE detections of STS are more reliable than MIPAS when compared to CALIPSO. The same observation can be made for ice.

4. Conclusion

This study compared the PSC composition measured using the absorption limb-viewing ACE instrument with nadir lidar observations (CALIPSO) and limb emission spectra (MIPAS). Different sets of coincidences between the satellites were considered.

CALIPSO and ACE comparisons were already carried out in a previous study [28] but the present work extends the comparison to almost the full length of the CALIPSO mission (2006-2020). Similar trends were found: excellent agreement for NAT, relatively good agreement for STS and poorer agreement for ice. Constraining the analysis to homogeneous clouds detected by CALIPSO improved significatively the agreement for STS and ice. This tends to show that the disagreement is partly due to spatial heterogeneity and the difference in spatial resolution between the satellites. SNA are consistently detected as STS by CALIPSO, and this is even more pronounced when considering homogeneous PSC scenes. This tend to show that sometimes CALIPSO is looking at large SNA clouds rather than STS clouds.

MIPAS and ACE comparisons yielded excellent agreement for NAT. This is not surprising as both instruments use a characteristic NAT feature at 820 cm^{-1}. For ice, the agreement between MIPAS

and ACE is relatively good, 45% of ACE ice is also detected as ice by MIPAS. The agreement for STS is not good; only 39% of ACE STS are detected as STS by MIPAS, almost all the rest are detected as NAT. The use by MIPAS of a single NAT spectroscopic feature could bias MIPAS toward NAT detection. The 820 cm^{-1} feature that MIPAS is using for detecting NAT corresponds to the ν_2-band of NO_3^-, however this band is not exclusively characteristic of NAT, in fact ACE observes this band (with less intensity) in SNA spectra, and STS spectra with high concentration of nitric acid. Disagreement between the two satellites could also be due to the sampling differences existing between solar occultation and limb emission. Triple coincidences show that the detection of STS by ACE is more reliable than that of MIPAS.

Overall, CALIPSO lidar has good spatial coverage; however, the composition is inferred based on particle shape and optical properties in the visible region. PSCs have no characteristic spectral features in the visible region. On the other hand, spectrometers like MIPAS and ACE do not have such good spatial coverage, but they rely on spectral features to identify the chemical composition. However, the spectral coverage of MIPAS is narrower than ACE and, for example, MIPAS misses the important OH stretching region near 3000 cm^{-1}. Absorption spectra of PSCs are also easier to interpret than emission spectra. ACE is shown in this study to give reliable PSC observations that are valuable in future polar winters, considering that MIPAS and CALIPSO are out of service.

CRediT authorship contribution statement

Léo Lavy: Investigation, Formal analysis, Visualization, Writing – original draft, review & editing. **Peter Bernath:** Investigation, Supervision, Writing – review & editing. **Michael Lecours:** Investigation, Data curation, Writing – review & editing. **Dylan English:** Investigation, Data curation, Writing – review & editing.

Data availability

Data will be made available on request.

Acknowledgement

The ACE mission is funded by the Canadian Space Agency (9F045-200575/001/SA). Some support was provided by NASA through the Atmospheric Composition Modeling and Analysis Program (80NSSC23K0999). PB acknowledges RB for productive discussion.

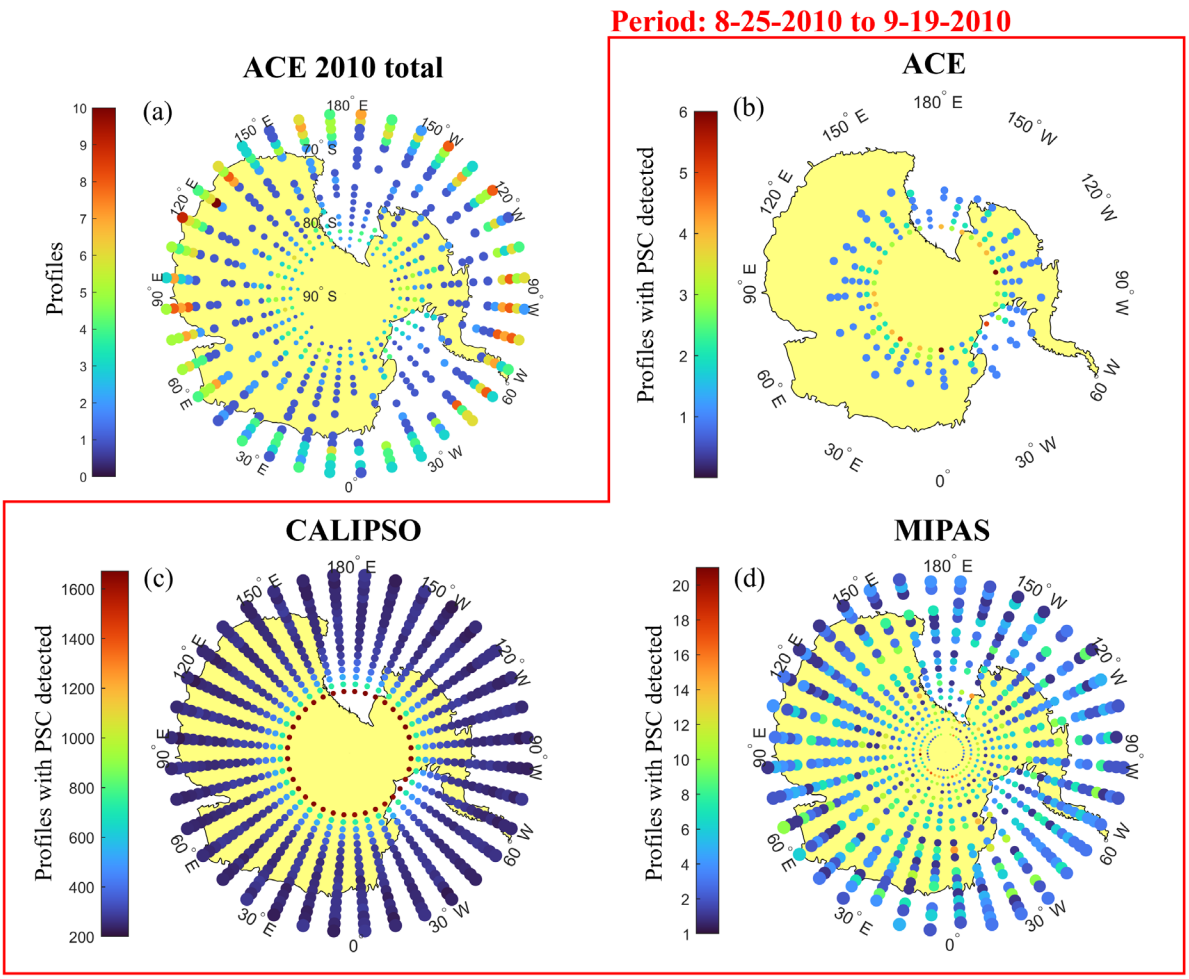

Fig. 1. (a): All ACE observations for 2010. (b): All ACE observations of PSCs considered in this paper for 2010, in the period 8-25-2010 to 9-19-2010. (c): For the same period, all CALIPSO profiles containing at least one PSC observation. (d): For the same period, all MIPAS profiles containing at least one PSC observation. Each dot represents a 10˚ longitude, 1˚ latitude region, with its size proportional to the area.

Year	CALIPSO-ACE Coincidences	Total ACE PSCs	ACE Ice-mixture	ACE NAT	ACE STS	ACE SNA	ACE NAT-STS
2006	96	450	83	39	122	0	206
2007	113	566	82	103	140	3	238
2008	116	557	111	85	75	0	286
2009	207	989	104	266	98	2	519
2010	235	953	64	75	157	12	645
2011	192	1004	169	366	105	2	362
2012	159	550	50	46	160	8	286
2013	208	755	90	43	274	4	344
2014	173	918	180	187	258	5	288
2015	233	892	131	25	325	2	409
2016	233	1011	54	111	483	1	362
2017	135	471	40	6	182	0	243
2018	173	1193	121	326	237	2	507
2019	197	331	42	27	66	4	192
2020	149	466	113	131	110	0	112
TOTAL	2619	11106	1434	1836	2792	45	4999

Tab. 1. CALIPSO-ACE coincidences found in the Antarctic for the period 2006-2020 with detailed counts of ACE PSCs and their composition ($\Delta t \leq 6$ hours and $\Delta d \leq 150$ km).

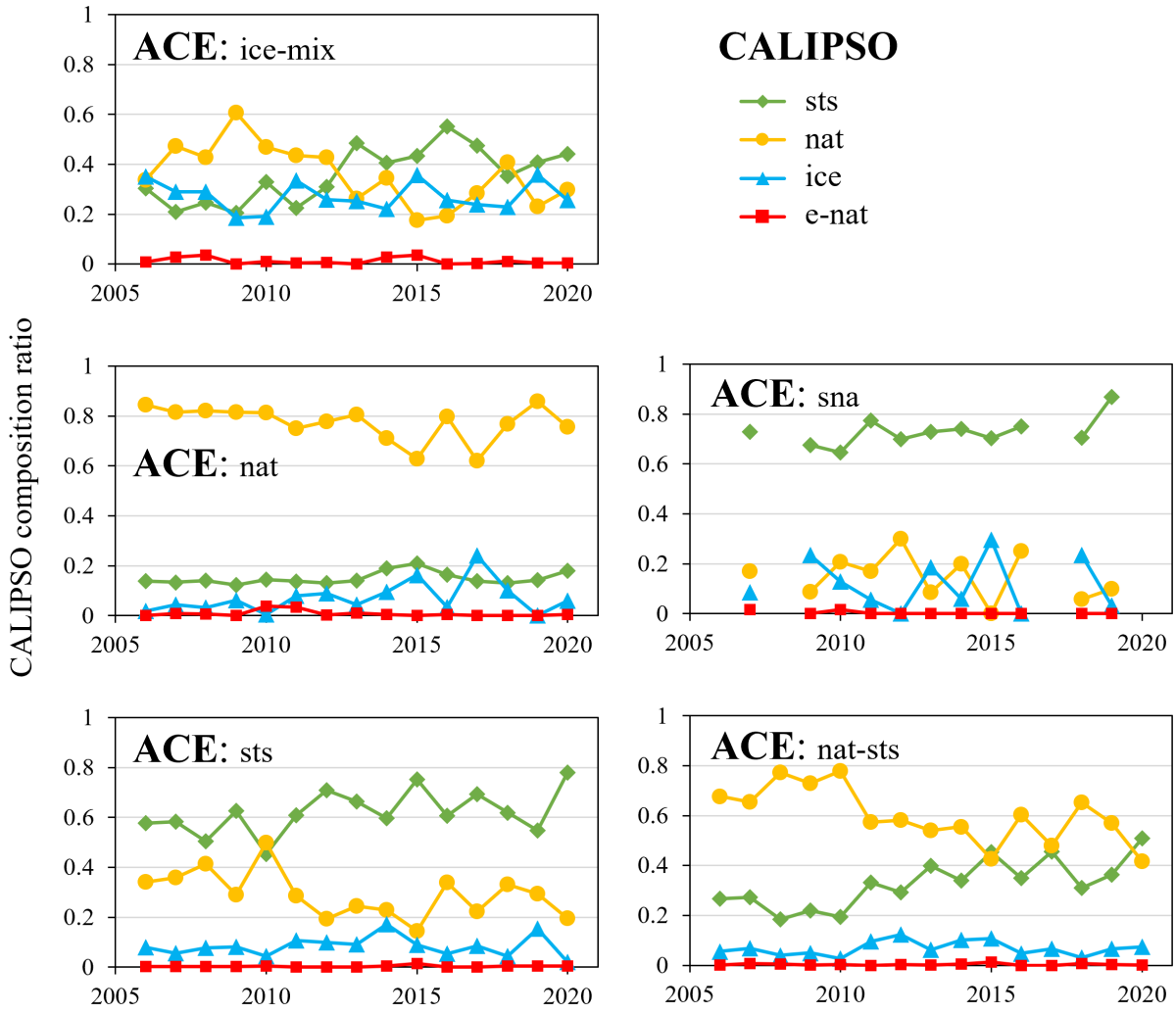

Fig. 2. Comparison between ACE and CALIPSO composition measurements for coincidences between the two satellites in the Antarctic as a function of the year. Each graph shows for a particular ACE composition the ratio of CALIPSO compositions when a PSC is detected. See Table 1 for information on the statistics for each year.

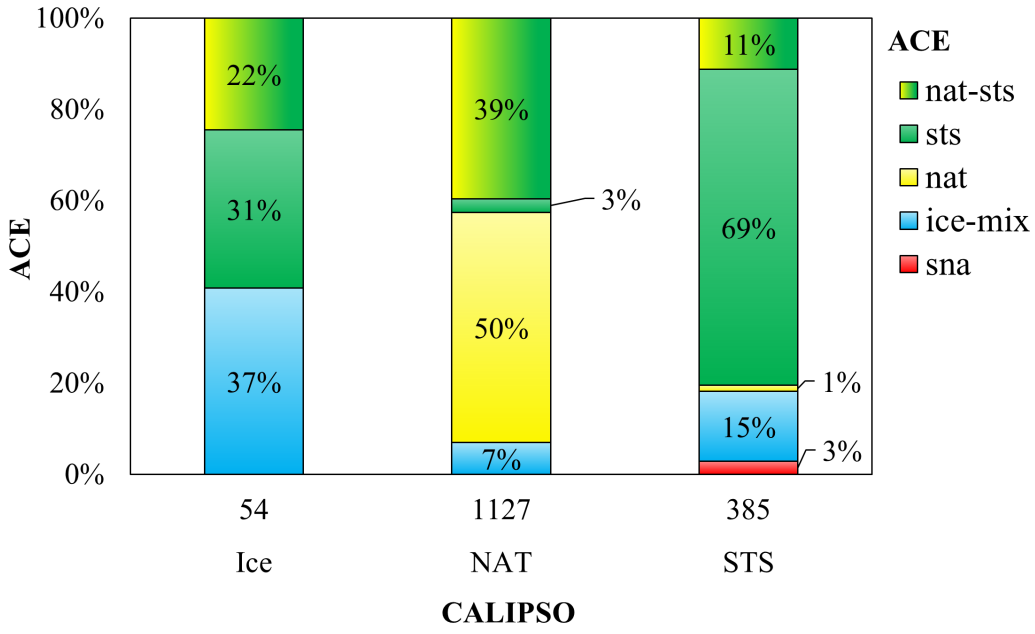

Fig. 3. Comparison of ACE and CALIPSO PSC composition for spatially homogeneous scenes measured by CALIPSO. The graph is made with a set of coincidences in the Antarctic in the period 2006-2020. The x-axis shows the total number of coincident detections for each CALIPSO composition, the y-axis shows the ACE composition.

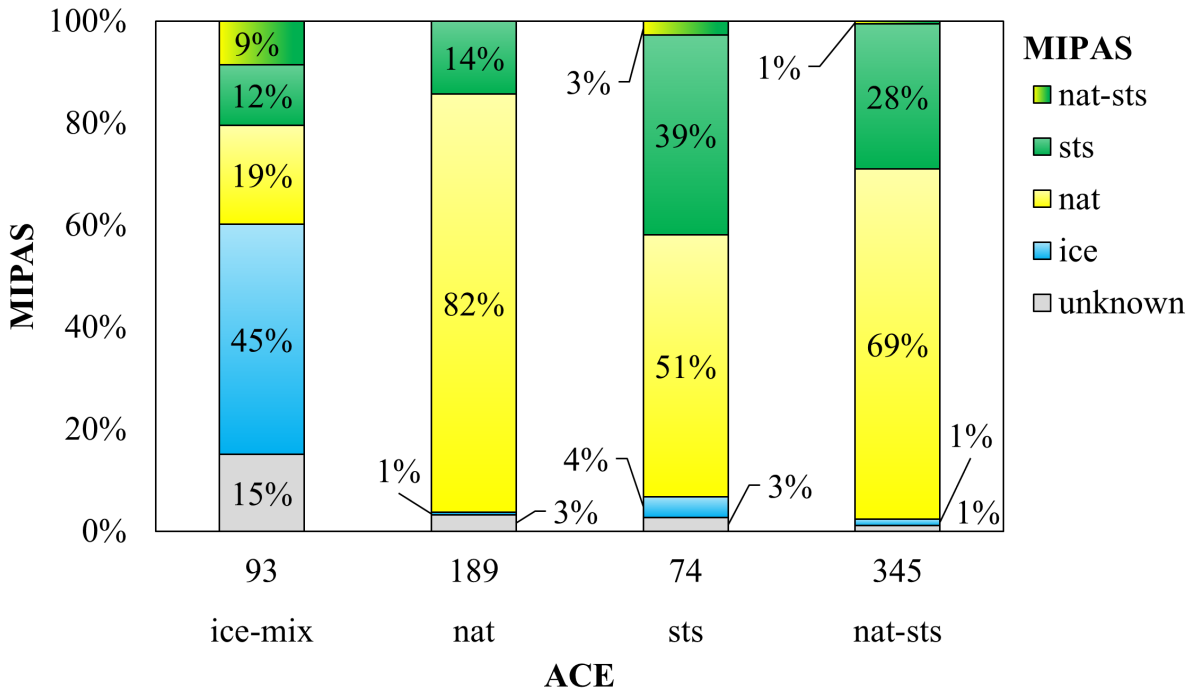

Fig. 4. Comparison of the ACE and MIPAS PSC composition for coincidences between the two satellites in the Antarctic in the period 2005-2011. The x-axis shows the total number of ACE detections and their composition, the y-axis shows the MIPAS composition, without considering no-cloud detections.

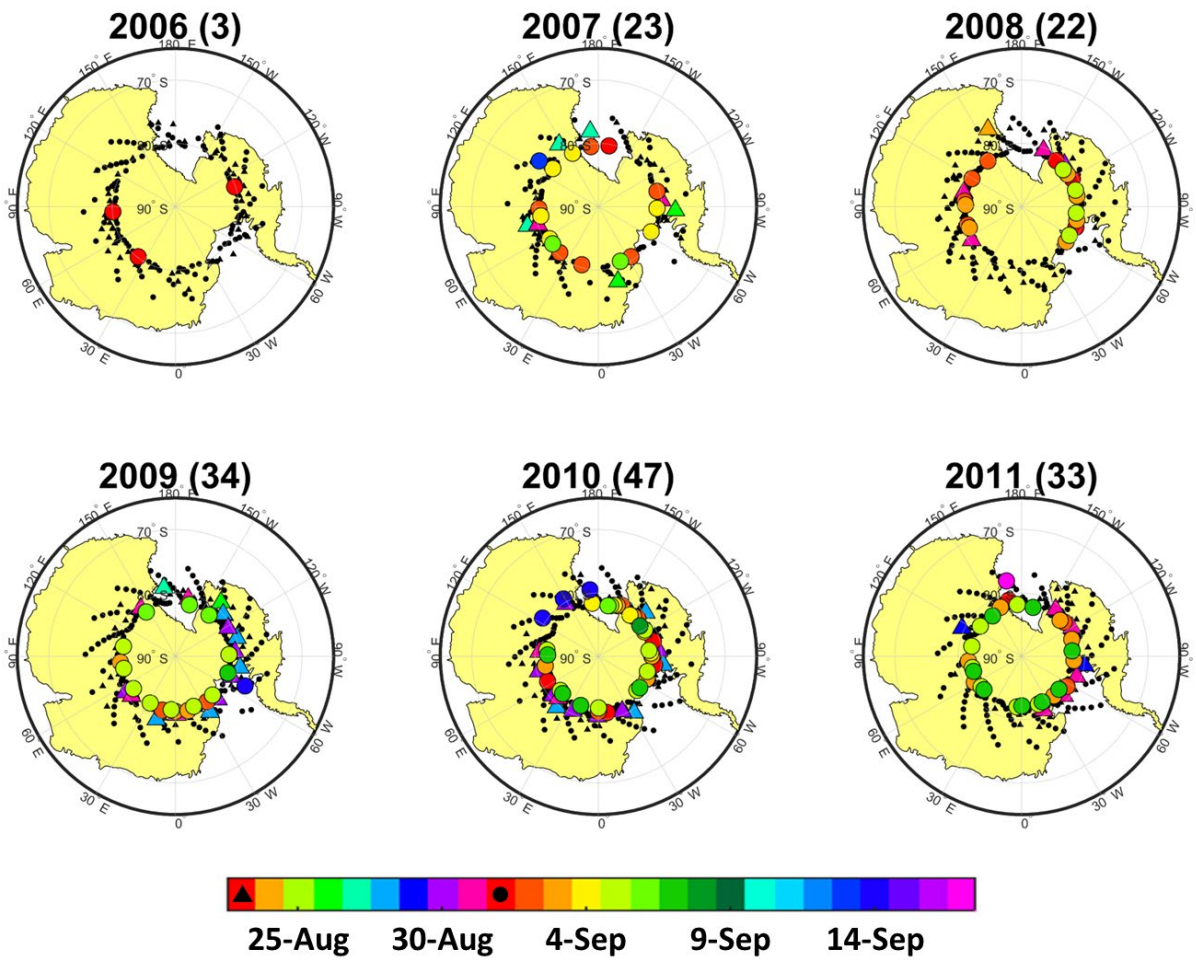

Fig. 5. Triple coincidences between 2006 and 2011 shown in maps of the Antarctic. The black markers show ACE observations, and the colored markers show ACE observations in coincidence with both CALIPSO and MIPAS ($\Delta t \leq$ 6 hours and $\Delta d \leq$ 150 km, relative to ACE). The number of these triple coincidences for each year is reported in parentheses in the titles. The color indicates the day of the year. The considered period in this study is restricted to observations in August (triangles) and September (circles).

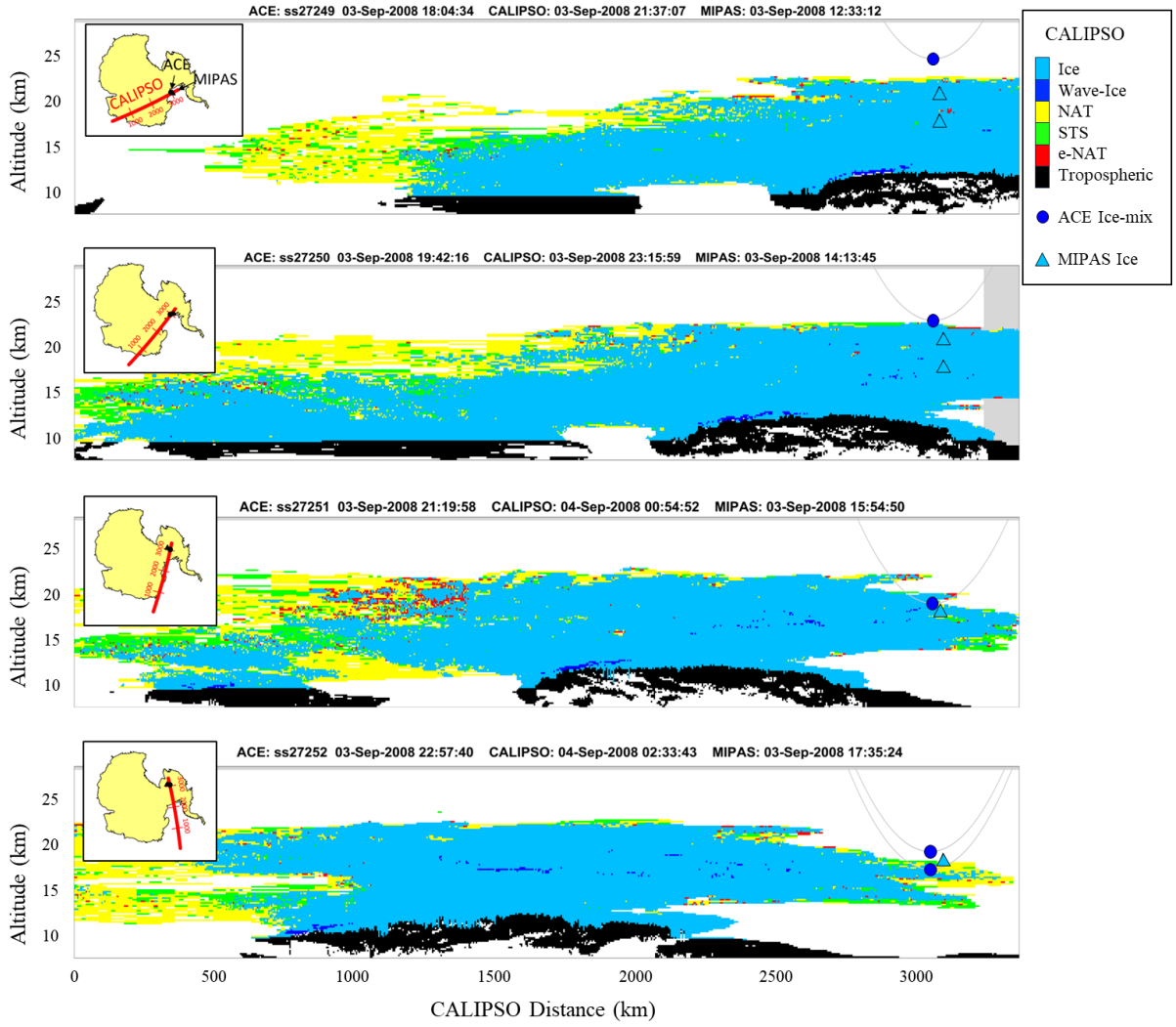

Fig. 6. Simultaneous detection of an ice cloud by the three satellites in September 2008. ACE detections in absorption spectroscopy (circles), MIPAS detections in emission spectroscopy (triangles) and CALIPSO lidar detections (background curtain). The grey curves associated with ACE detections show the line-of-sight of the satellite, assuming it is in the plane of the CALIPSO curtain. Positions of detections are shown in a map of Antarctica in the insert with the CALIPSO ground track shown in red.

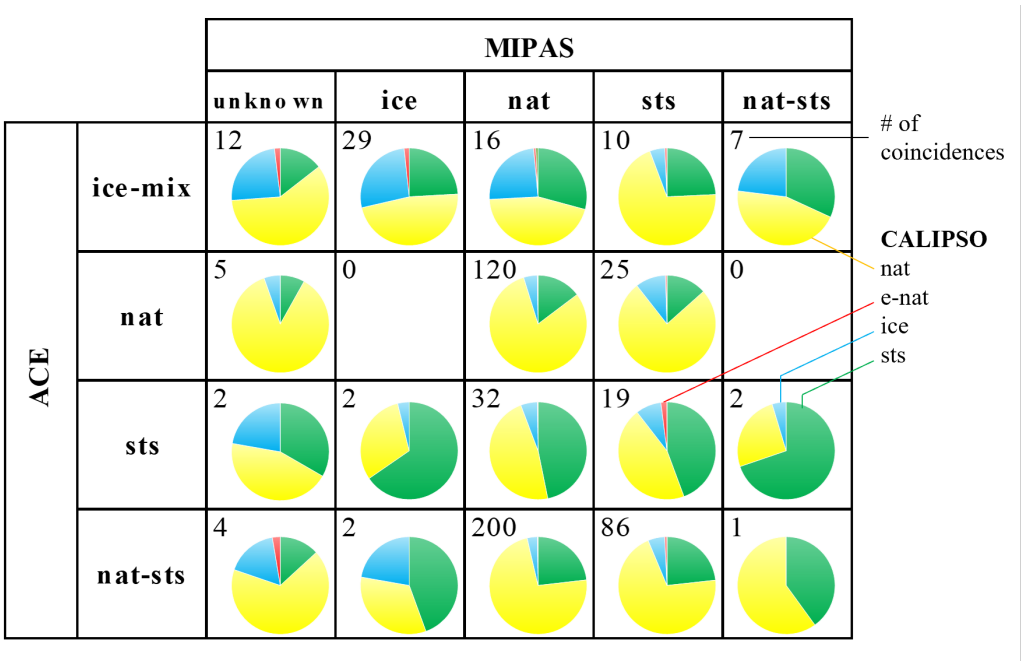

Fig. 7. Triple coincidences: comparison between ACE, MIPAS and CALIPSO. The table shows for each ACE-MIPAS composition pair, the composition measured by CALIPSO in coincidence as a pie chart. The total number of ACE-MIPAS coincidences is shown in the top right corners. The pie charts consider all the CALIPSO observations within a 4 km vertical window of ACE.

References

[1] Lowe D, MacKenzie AR. Polar stratospheric cloud microphysics and chemistry. J Atmos Sol-Terr Phys. 2008;70(1):13-40. doi:10.1016/j.jastp.2007.09.011.

[2] Tritscher I, Pitts MC, Poole LR, Alexander SP, Cairo F, Chipperfield MP, et al. Polar stratospheric clouds: satellite observations, processes, and role in ozone depletion. Rev Geophys. 2021;59(2). doi:10.1029/2020RG000702.

[3] Molina MJ, Rowland FS. Stratospheric sink for chlorofluoromethanes: chlorine atom-catalysed destruction of ozone. Nature. 1974;249(5460):810-812. doi:10.1038/249810a0.

[4] Solomon S. Stratospheric ozone depletion: A review of concepts and history. Rev Geophys. 1999;37(3):275-316. doi:10.1029/1999RG900008.

[5] Farman JC, Gardiner BG, Shanklin JD. Large losses of total ozone in Antarctica reveal seasonal ClO_x/NO_x interaction. Nature. 1985;315:207-210. doi:10.1038/315207a0.

[6] Solomon S, Garciat RR, Rowland FS, Wuebbles DJ. On the depletion of Antarctic ozone. Nature. 1986;321:755-758. doi:10.1038/321755a0.

[7] Lambert A, Santee ML, Wu DL, Chae JH. A-train CALIOP and MLS observations of early winter Antarctic polar stratospheric clouds and nitric acid in 2008. Atmos Chem Phys. 2012;12(6):2899-2931. doi:10.5194/acp-12-2899-2012.

[8] Burkholder JB, Sander SP, Abbatt J, Barker JR, Cappa C, Crounse JD, et al. Chemical kinetics and photochemical data for use in atmospheric studies, evaluation No. 19, Pasadena: Jet Propulsion Laboratory; 2019. JPL Publication 19-5. http://jpldataeval.jpl.nasa.gov.

[9] Carslaw KS, Peter T, Clegg SL. Modeling the composition of liquid stratospheric aerosols. Rev Geophys. 1997;35(2):125-154. doi:10.1029/97RG00078.

[10] Müller R, Grooß JU, Zafar AM, Robrecht S, Lehmann R. The maintenance of elevated active chlorine levels in the Antarctic lower stratosphere through HCl null cycles. Atmos Chem Phys. 2018;18(4):2985-2997. doi:10.5194/acp-18-2985-2018.

[11] Grooß JU, Müller R, Spang R, Tritscher I, Wegner T, Chipperfield MP, et al. On the discrepancy of HCl processing in the core of the wintertime polar vortices. Atmos Chem Phys. 2018;18(12):8647-8666. doi:10.5194/acp-18-8647-2018.

[12] Murphy DM, Froyd KD, Schwarz JP, Wilson JC. Observations of the chemical composition of stratospheric aerosol particles. QJR Meteorol Soc. 2014;140(681):1269-1278. doi:10.1002/qj.2213.

[13] Molleker S, Borrmann S, Schlager H, Luo B, Frey W, Klingebiel M, et al. Microphysical properties of synoptic-scale polar stratospheric clouds: in situ measurements of unexpectedly large HNO_3-containing particles in the Arctic vortex. Atmos Chem Phys. 2014;14(19):10785-10801. doi:10.5194/acp-14-10785-2014.

[14] Voigt C. In situ mountain-wave polar stratospheric cloud measurements: implications for nitric acid trihydrate formation. J Geophys Res. 2003;108(D5):8331. doi:10.1029/2001JD001185.

[15] Tencé F, Jumelet J, Bouillon M, Cugnet D, Bekki S, Safieddine S, et al. 14 years of lidar measurements of polar stratospheric clouds at the French Antarctic station Dumont d'Urville. Atmos Chem Phys. 2023;23(1):431-451. doi:10.5194/acp-23-431-2023.

[16] Snels M, Scoccione A, Di Liberto L, Colao F, Pitts M, Poole L, et al. Comparison of Antarctic polar stratospheric cloud observations by ground-based and space-borne lidar and relevance for chemistry–climate models. Atmos Chem Phys. 2019;19(2):955-972. doi:10.5194/acp-19-955-2019.

[17] Snels M, Colao F, Cairo F, Shuli I, Scoccione A, De Muro M, et al. Quasi-coincident observations of polar stratospheric clouds by ground-based lidar and CALIOP at Concordia (Dome C, Antarctica) from 2014 to 2018. Atmos Chem Phys. 2021;21(3):2165-2178. doi:10.5194/acp-21-2165-2021.

[18] Spang R, Hoffmann L, Müller R, Grooß JU, Tritscher I, Höpfner M, et al. A climatology of polar stratospheric cloud composition between 2002 and 2012 based on MIPAS/Envisat observations. Atmos Chem Phys. 2018;18(7):5089-5113. doi:10.5194/acp-18-5089-2018.

[19] Pitts MC, Poole LR, Gonzalez R. Polar stratospheric cloud climatology based on CALIPSO spaceborne lidar measurements from 2006 to 2017. Atmos Chem Phys. 2018;18(15):10881-10913. doi:10.5194/acp-18-10881-2018.

[20] Lecours M, Boone CD, Bernath PF. Polar stratospheric cloud analysis of ACE data from 2005 to 2023. J Geophys Res: Atmos. 2024;Submitted.

[21] Lecours M, Bernath P, Boone C, Crouse J. Infrared transmittance spectra of polar stratospheric clouds. J Quant Spectrosc Radiat Transf. 2023;294:108406. doi:10.1016/j.jqsrt.2022.108406.

[22] Kim Y, Choi W, Lee KM, Park JH, Massie ST, Sasano Y, et al. Polar stratospheric clouds observed by the ILAS-II in the Antarctic region: Dual compositions and variation of compositions during June to August of 2003. J Geophys Res. 2006;111(D13):D13S90. doi:10.1029/2005JD006445.

[23] McCormick MP, Steele HM, Hamill P, Chu WP, Swissler TJ. Polar Stratospheric Cloud Sightings by SAM II. J Atmos Sci. 1982;39(6):1387-1397. doi:10.1175/1520-0469(1982)039<1387:PSCSBS>2.0.CO;2

[24] Pitts MC, Poole LR, McCormick MP. SAGE II observations of polar stratospheric clouds near 50°N January 31–February 2, 1989. Geophys Res Lett. 1990;17(4):405-408. doi:10.1029/GL017i004p00405

[25] Poole LR, Trepte CR, Harvey VL, Toon GC, VanValkenburg RL. SAGE III observations of Arctic polar stratospheric clouds – December 2002. Geophys Res Lett. 2003;30(23):2003GL018496. doi:10.1029/2003GL018496

[26] Fromm MD, Lumpe JD, Bevilacqua RM, Shettle EP, Hornstein J, Massie ST, et al. Observations of Antarctic polar stratospheric clouds by POAM II: 1994–1996. J Geophys Res. 1997;102(D19):23659-23672. doi:10.1029/97JD00794

[27] Benson CM, Drdla K, Nedoluha GE, Shettle EP, Alfred J, Hoppel KW. Polar stratospheric clouds in the 1998–2003 Antarctic vortex: Microphysical modeling and Polar Ozone and Aerosol Measurement (POAM) III observations. J Geophys Res. 2006;111(D18):2005JD006948. doi:10.1029/2005JD006948

[28] Lavy L, Bernath P, Lecours M, English D, Fromm M. Comparison between ACE and CALIPSO observations of Antarctic polar stratospheric clouds. J Quant Spectrosc Radiat Transf. 2024;313:108827. doi:10.1016/j.jqsrt.2023.108827.

[29] Bernath PF. The Atmospheric Chemistry Experiment (ACE). J Quant Spectrosc Radiat Transf. 2017;186:3-16. doi:10.1016/j.jqsrt.2016.04.006.

[30] Boone CD, Bernath PF, Cok D, Jones SC, Steffen J. Version 4 retrievals for the atmospheric chemistry experiment Fourier transform spectrometer (ACE-FTS) and imagers. J Quant Spectrosc Radiat Transf. 2020;247:106939. doi:10.1016/j.jqsrt.2020.106939.

[31] Bernath PF, Crouse J, Hughes RC, Boone CD. The Atmospheric Chemistry Experiment Fourier transform spectrometer (ACE-FTS) version 4.1 retrievals: Trends and seasonal distributions. J Quant Spectrosc Radiat Transf. 2021;259:107409. doi:10.1016/j.jqsrt.2020.107409.

[32] Gordon IE, Rothman LS, Hargreaves RJ, Hashemi R, Karlovets EV, Skinner FM, et al. The HITRAN2020 molecular spectroscopic database. J Quant Spectrosc Radiat Transf. 2022;277:107949. doi:10.1016/j.jqsrt.2021.107949.

[33] Lecours MJ, Bernath PF, Sorensen JJ, Boone CD, Johnson RM, LaBelle K. Atlas of ACE spectra of clouds and aerosols. J Quant Spectrosc Radiat Transf. 2022;292:108361. doi:10.1016/j.jqsrt.2022.108361.

[34] Boone CD, Bernath PF, Lecours M. Version 5 retrievals for ACE-FTS and ACE-imagers. J Quant Spectrosc Radiat Transf. 2023;310:108749. doi:10.1016/j.jqsrt.2023.108749.

[35] Stephens GL, Vane DG, Boain RJ, Mace GG, Sassen K, Wang Z, et al. THhe CLOUDSAT mission and the A-train: a new dimension of space-based observations of clouds and precipitation. Bull Amer Meteor Soc. 2002;83(12):1771-1790. doi:10.1175/BAMS-83-12-1771.

[36] Winker DM, Vaughan MA, Omar A, Hu Y, Powell KA, Liu Z, et al. Overview of the CALIPSO mission and CALIOP data processing algorithms. J Atmos Ocean Technol. 2009;26(11):2310-2323. doi:10.1175/2009JTECHA1281.1.

[37] Pitts MC, Thomason LW, Poole LR, Winker DM. Characterization of polar stratospheric clouds with spaceborne lidar: CALIPSO and the 2006 Antarctic season. Atmos Chem Phys. 2007;7(19):5207-5228. doi.org/10.5194/acp-7-5207-2007.

[38] Pitts MC, Poole LR, Thomason LW. CALIPSO polar stratospheric cloud observations: second-generation detection algorithm and composition discrimination. Atmos Chem Phys. 2009;9(19):7577-7589. doi.org/10.5194/acp-9-7577-2009.

[39] Pitts MC, Poole LR, Dörnbrack A, Thomason LW. The 2009–2010 Arctic polar stratospheric cloud season: a CALIPSO perspective. Atmos Chem Phys. 2011;11(5):2161-2177. doi:10.5194/acp-11-2161-2011.

[40] Pitts MC, Poole LR, Lambert A, Thomason LW. An assessment of CALIOP polar stratospheric cloud composition classification. Atmos Chem Phys. 2013;13(6):2975-2988. doi:10.5194/acp-13-2975-2013.

[41] Fischer H, Birk M, Blom C, Carli B, Carlotti M, Endemann M, et al. MIPAS: an instrument for atmospheric and climate research. Atmos Chem Phys. 2008;8(8):2151-2188. doi.org/10.5194/acp-8-2151-2008.

[42] Spang R, Remedios JJ. Observations of a distinctive infra-red spectral feature in the atmospheric spectra of polar stratospheric clouds measured by the CRISTA instrument. Geophys Res Lett. 2003;30(16):1875. doi:10.1029/2003GL017231.

[43] Spang R, Remedios JJ, Kramer LJ, Poole LR, Fromm MD, Konopka P. Polar stratospheric cloud observations by MIPAS on ENVISAT: detection method, validation and analysis of the northern hemisphere winter 2002/2003. Atmos Chem Phys. 2005;5(3):679-692. doi.org/10.5194/acp-5-679-2005.

[44] Spang R, Arndt K, Dudhia A, Höpfner M, Hoffmann L, Hurley J, et al. Fast cloud parameter retrievals of MIPAS/Envisat. Atmos Chem Phys. 2012;12(15):7135-7164. doi:10.5194/acp-12-7135-2012.

[45] Spang R, Hoffmann L, Höpfner M, Griessbach S, Müller R, Pitts MC, et al. A multi-wavelength classification method for polar stratospheric cloud types using infrared limb spectra. Atmos Meas Tech. 2016;9(8):3619-3639. doi:10.5194/amt-9-3619-2016.

[46] Hoffmann L, Spang R, Orr A, Alexander MJ, Holt LA, Stein O. A decadal satellite record of gravity wave activity in the lower stratosphere to study polar stratospheric cloud formation. Atmos Chem Phys. 2017;17(4):2901-2920. doi:10.5194/acp-17-2901-2017.

[47] MIPAS/Envisat observations of polar stratospheric clouds. Re3data.Org. doi:10.17616/R3BN26.